

The CAST Time Projection Chamber

D Autiero^{1,‡}, B Beltrán², J M Carmona³, S Cebrián³, E Chesi¹,
 M Davenport¹, M Delattre¹, L Di Lella^{1,§}, F Formenti¹,
 I G Irastorza^{1,||}, H Gómez³, M Hasinoff⁴, B Lakić⁵, G Luzón³,
 J Morales³, L Musa¹, A Ortiz³, A Placci¹, A Rodriguez³,
 J Ruz³, J A Villar³ and K Zioutas^{1,6}

¹ European Organization for Nuclear Research (CERN), CH-1211 Genève 23, Switzerland

² Department of Physics, Queen's University, Kingston, Ontario K7L 3N6, Canada

³ Laboratorio de Física Nuclear y Altas Energías, Universidad de Zaragoza, Zaragoza, Spain

⁴ Department of Physics and Astronomy, University of British Columbia, Vancouver, Canada

⁵ Rudjer Bošković Institute, Zagreb, Croatia

⁶ University of Patras, Patras, Greece

E-mail: jaime.ruz@cern.ch

Abstract. One of the three X-ray detectors of the CAST experiment searching for solar axions is a Time Projection Chamber (TPC) with a multi-wire proportional counter (MWPC) as a readout structure. Its design has been optimized to provide high sensitivity to the detection of the low intensity X-ray signal expected in the CAST experiment. A low hardware threshold of 0.8 keV is safely set during normal data taking periods, and the overall efficiency for the detection of photons coming from conversion of solar axions is 62%. Shielding has been installed around the detector, lowering the background level to $4.10 \times 10^{-5} \text{ counts cm}^{-2} \text{ s}^{-1} \text{ keV}^{-1}$ between 1 and 10 keV. During phase I of the CAST experiment the TPC has provided robust and stable operation, thus contributing with a competitive result to the overall CAST limit on axion-photon coupling and mass.

PACS numbers: 29.40.Cs, 95.35.+d, 07.85.Nc, 07.05.Fb, 07.05.Kf

Submitted to: *New J. Phys.*

‡ Present addr.: Inst. de Physique Nucléaire, Lyon, France.

§ Present addr.: Scuola Normale Superiore, Pisa, Italy.

|| Present addr.: DAPNIA, Centre d'Études Nucléaires de Saclay (CEA-Saclay), Gif-sur-Yvette, France.

1. Introduction

The CERN Solar Axion Telescope (CAST) is the most sensitive implementation of the “helioscope” concept to look for hypothetical axions (or axion-like particles) coming from the Sun (Sikivie 1983). CAST makes use of a decommissioned LHC prototype magnet with a length of 9.3 m, providing a 9 Tesla field to trigger the conversion of solar axions into X-rays, which can then be detected by the three different X-ray detectors placed at both ends of the magnet (Zioutas et al. 1999). The purpose of the present paper is to describe one of the detector systems of CAST: the time projection chamber (TPC). Accompanying papers are devoted to the other two X-ray detectors (Kuster et al. 2007, Abbon et al. 2007) as well as to an overall description of the experiment (Andriamonje et al. 2007). The first physics results of CAST phase I have been published in Zioutas et al. (2005) and Andriamonje et al. (2007).

The TPC detector is attached to eastern end of the CAST magnet, covering both magnet bores and being therefore exposed to the converted photons from “sunset” axions during evening solar tracking. The design of the detector follows the well-known concept of a conventional TPC, i.e., a large volume gaseous space where primary interactions take place, producing ionization electrons which drift towards a plane of wires. Here, as in a Multi Wire Proportional Chamber (MWPC), the avalanche process that amplifies the signal is developed, allowing a position sensitive readout of the original event. The specific requirements of the CAST experiment (sensitivity to a low intensity X-ray signal peaking at ~ 4 keV and vanishing at around 10 keV), necessitated some original approaches in the construction of the CAST TPC. An optimum performance would include: low threshold (at the keV level), a relatively high gain, position sensitivity (to distinguish events coming from the magnet bores and to allow some degree of background rejection by pattern recognition), good efficiency for the energies of interest, low background at low energies, and last but not least, robust and stable operation over the long data taking periods needed to accumulate enough statistics. The CAST TPC was designed to fulfill these requirements using conventional reliable technology.

Our paper is structured as follows: in section 2 description of the detector itself and the shielding installed is given. It is followed by a description of the data acquisition electronics in section 3 and the characterization of the detector based on the calibration data at the PANTER X-ray test facility in Munich in section 4. Finally, the basic data treatment is described in section 5, stressing the aspects concerning offline background strategies and the detector performance during data taking period of CAST phase I will be presented in section 6.

2. Chamber and Shielding Concept

2.1. Chamber Description

The CAST TPC has a conversion volume of $10 \times 15 \times 30$ cm³. The 10 cm drift direction is parallel to the magnet beam pipes, and the section of 15×30 cm² is

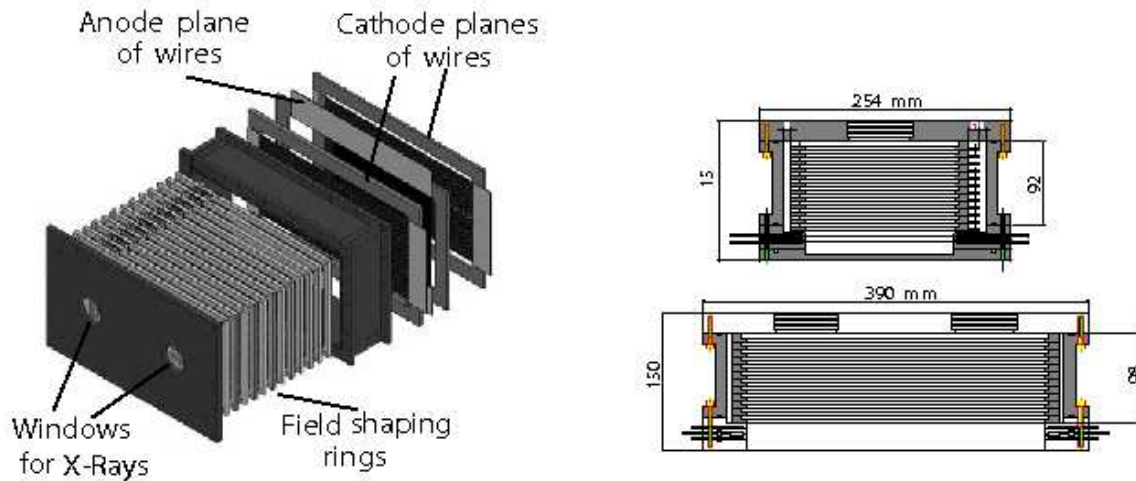


Figure 1. Left: Exploded view of the TPC. The pieces holding the anode and cathode wire planes and the field shaping conductive frames are clearly seen. The holes to hold the circular windows for the X-rays coming out from the magnet bores are present in the front piece. Right: Both side views of the TPC showing the general dimensions in millimeters.

perpendicular to that direction, covering both magnet bores (each bore has a diameter of 42 mm and their centers are separated by 18 cm). This conversion volume, filled with gas Ar(95%)/CH₄(5%) at atmospheric pressure, allows for essentially total conversion (> 99%) of photons up to 6 keV crossing the chamber parallel to the magnet beam direction. The conversion efficiency decreases for higher energies, becoming 50% for photons of 11.5 keV. The gas is being continuously renewed at a flow rate of 2 l h⁻¹, in order to prevent any contamination from atmospheric impurities, such as N₂ or O₂.

The maximum drift distance is 10 cm between the drift electrode and the sense wires. The drift electrode is a continuous aluminum layer located on the inner side of the chamber wall closer to the magnet, extended to its whole 15 × 30 cm² dimension. It is biased at -7 kV, thereby producing an electric field of 700 V cm⁻¹. To shape the electric field at the chamber edges, several rectangular (15 × 30 cm²) conductive frames at intermediate voltages stepping between 0 and -7 kV are used (see figure 1). On the back side of the chamber, the wires are arranged in 3 planes, one anode plane at +1.8 kV between two grounded cathode planes. The anode plane contains 48 wires of 20 μm diameter (gold plated tungsten) which run parallel to the wider side of the chamber. Each cathode plane contains 96 wires of 100 μm diameter that run perpendicular to the anode wires. The intense electric field surrounding the anode (sense) wires causes the avalanche process and hence the multiplication of the primary ionization cloud. The positive ions produced in an avalanche event are cleared away by the neighboring cathode wires, which receive an induced signal, providing two dimensional information

for each event. The distance between adjacent wires of the same plane is 3 mm. The distance between the anode and the cathode plane closest to the drift region is 3 mm, while the distance between the anodes and the outer cathode plane is 6 mm. This asymmetric configuration enhances the induced signal on the cathode wires closest to the drift region, which are the ones read out by the electronics. As a result, the ratio between the anode and cathode signals for a given energy deposition in the chamber, a parameter purely determined by geometry, is approximatively a factor of 2 in our case.

With the exception of the electrodes themselves, plus the screws and the Printed Circuit Board (PCB) where the wires are held, the entire chamber is made of plexiglass. The radioactivity level of this material has been measured at the Canfranc Underground Laboratory facility and found to be very low ($< 100 \text{ mBq kg}^{-1}$ of ^{238}U , $< 10 \text{ mBq Kg}^{-1}$ of ^{235}U , $< 5 \text{ mBq kg}^{-1}$ of ^{232}Th and $< 30 \text{ mBq kg}^{-1}$ of ^{40}K) therefore suitable for our low background application. The thickness of the plexiglass wall is about 1.7 cm, except in three places (two on the back side and one on a lateral side) where the only separation between the inner gas and the atmosphere is a thin mylar foil to allow the calibration of the chamber with low energy X-ray sources. In addition, the side closet to the magnet has two 6 cm radius circular holes for the thin windows that must be as transparent as possible to the X-rays coming through the magnet, while being able to hold the large pressure difference (1 atm) between the chamber gas and the magnet bore.

These windows are basically very thin mylar foils (3 or 5 μm) stretched, then glued to a metallic grid (strongback) on the vacuum side of the foil. This technique allows the thin foil to withstand the large pressure difference. The geometrical opacity of the strongback is about 8% while the mylar foil is practically transparent for X-rays down to the keV energies ($\sim 30\%$ transparency for 1 keV, $\sim 85\%$ for 2 keV and $\sim 95\%$ for 3 keV, see Henke et al. 1993). The inner side of the mylar foil is aluminized (40 nm) since it serves as part of the drift electrode. To minimize the effect of the chamber gas leaks towards the magnet, and therefore to cope with the stringent requirements of the magnet vacuum system, a differential pumping system has been installed. This system creates an intermediate volume between the TPC and the magnet which is continuously being pumped with a clean pump. This volume is kept at a relatively poor vacuum ($\sim 10^{-5}$ mbar, compared with $\sim 10^{-7}$ mbar in the magnet). A second thin polypropylene window separates this intermediate volume from the magnet vacuum. Due to the small pressure difference, the effective leak through this window is extremely small (1.46×10^{-7} mbar ls^{-1} of Argon). This strategy allows us to be reasonably tolerant to small leaks on the TPC windows, improving the robustness of the whole system.

2.2. Background Sources and Shielding Concept

The CAST experiment is located in one of the surface buildings of the PA8 experimental area at CERN. Due to the fact that the TPC is attached to the end of the magnet which is far from the pivot point, it moves not only over relatively large distances during each daily solar tracking but also shifts position within the hall progressively following the

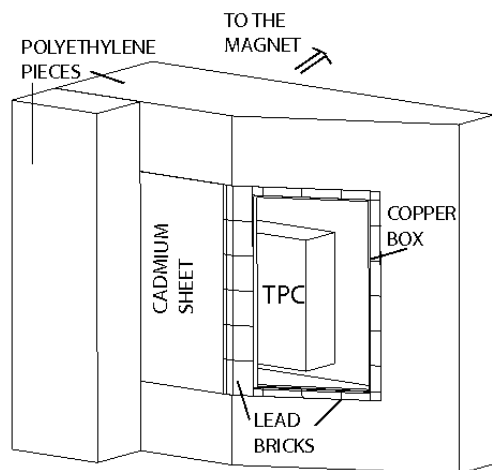


Figure 2. Shielding scheme showing all the layers that surround the TPC, from the inside to the outside: a copper box, a lead , cadmium, and polyethylene shield.

seasons. If the spatial distribution of possible background sources is not uniform in the hall, this movement may induce background fluctuations in the detector.

To assess possible sources of background for the TPC, one has to take into account the high event discrimination capabilities of the TPC. Most of the events contributing to the raw trigger rate are muons and other cosmic-ray related, multi-cluster (or track) events, and they are easily rejected by the software cuts described in section 5. In the following, we denote as background only those events which survive the cuts, i.e., which leave a single point-like energy deposition in the detector.

Events which contribute to this remaining background are photons induced by cosmic rays in the surrounding materials or produced by the radioactive chains and potassium in laboratory floor, building and experimental materials (Dumont 2004). The TPC detector is practically blind to most of this high energy radiation, but low energy Compton interactions in the detector are still possible. Also, their interaction in the surrounding materials can produce a diffuse gamma background of lower energies, with a high probability of interacting in the gas. These components depend on the concentration of the original emitters in the laboratory floor and walls and, in general, on the geometry of the detector environment, therefore causing a non-uniform background. Radon is also present everywhere and its concentration has been measured to vary widely between 5 and 50 Bq m⁻³ depending on causes such as walls or floor proximity, ventilation, and the atmospheric pressure, temperature and humidity. The neutron component of the background is below the level of the typical gamma background by three or four orders of magnitude, but neutron signal in the detector could mimic those from X-rays. The dominant sources of this background are cosmic rays, but neutrons can be also induced by muons in surrounding materials, by (α , n) reactions on light elements and by spontaneous fission.

In view of these general considerations, a shielding around the TPC was designed not only to reduce the general level of background seen by the detectors, but also to homogenize its position dependence. The final design is the outcome of several simulations and experimental tests, some of which have been performed in the actual TPC to assess the effect of the shielding on the detector background data (Ruz & Luzón 2006). Also a compromise was to be found between the shielding effect and the weight and size restrictions imposed by the limitations of the lifting screws and support structure. From the inside to outside, the CAST TPC shielding (see figure 2) is composed of:

- Copper box, 5 mm thick: it reduces the electronic noise, as a Faraday cage, and stops low energy X-rays produced in the outer part of the shielding by environmental gamma radiation. It is also used for mechanical support purposes.
- Lead wall, 2.5 cm thick: To reduce the low and medium energy environmental gamma radiation.
- Cadmium layer, 1 mm thick: to absorb the thermal neutrons slowed down by the outer polyethylene wall.
- Polyethylene wall, 22.5 cm thick: to slow the medium energy environmental neutrons down to thermal energies.
- PVC bag: to cover the whole shielding assembly. This tightly closes the entire set-up allowing to flush the inner part with pure N₂ gas (coming from liquid nitrogen evaporation) at an average rate of 250 l h⁻¹, in order to remove radon from this space.
- Scintillating veto: placed at the top of the shielding, a scintillating plastic of 80 × 40 × 5 cm³ is placed to reject muon-induced events by anti-coincidence with the detector.

3. Data Acquisition Hardware and Software

The first stage of wire signal amplification and shaping is performed by 36 (12 for the anodes and 24 for the cathodes) ALCATEL SMB302 4-channel preamplifier chips, located on the same printed circuit board on which the wires are supported. The output from these preamplifiers is sampled by three 48-channel 10-bit VME flash-ADCs operating at a sampling rate of 10 MHz. These modules are based on the ALTRO (ALICE TPC Read-Out) chip, developed at CERN for the ALICE experiment (Bosch 2003). The same modules have been used in the HARP and CERES (NA45) experiments at CERN.

The trigger is built from the OR of all the anode signals. The hardware trigger threshold during normal CAST data-taking operation is safely set to avoid being triggered by electronic noise, and corresponds to energy depositions of about 800 eV in the gas conversion region. The time window for the sampling is about 7 μs, which is long enough to encompass the maximum drift time of the chamber. The flash-ADCs

are configured, controlled and read through a VME bus controlled by a dual processor PC running under Linux, which uses a SBS Bit-3 1003 adapter on a fiber-optic link.

The time spent by the system after the trigger arrival in hardware-processing the data, transferring them to the PC and writing them to the disk is, on average, about 1.5 ms, during which it is “blind” to new triggers. This means that for the typical chamber trigger rate of 10 to 25 Hz –depending of data taking conditions– the average dead time can vary from 1.75% to 2.5%. The dead time is continuously monitored by measuring the time the system spends in the “BUSY” state, defined by a hardware register which is set by the trigger and reset to zero by the PC once the event processing is finished. The BUSY logic is handled by a CORBO VME module. The dead time is therefore calculated on-line by using a scaler to count clock pulses both with and without a veto from the BUSY signal provided by the CORBO module.

The acquisition software is a low level C-code which configures, initializes and controls the electronics modules through the VME bus. Once a trigger is detected, its task is basically to dump the contents of the flash-ADC memories onto the disk, without any further data treatment, so as not to add any dead time. A different, high level C-code for passive monitoring of the detector performance is running continuously in the second processor, without interfering with the acquisition (and therefore without adding noticeable dead time). This software, based on the ROOT toolkit developed for data analysis at CERN (Brun & Rademakers 1996), monitors online multiple experimental parameters, and therefore allows fast diagnosis of problems and helps in assessing the quality of the data as they are being acquired.

The data acquisition protocol follows a fully automatic procedure, and data belonging to Sun-tracking (“axion-sensitive”) measurements or to background measurements are identified and separated during the off-line analysis (by using the slow control data). Therefore, the acquisition starts and stops are set only by practical reasons, mainly to allow a calibration of the detector. The gain of the detector is measured using a ^{55}Fe source and the pedestal levels and the variation of the flash-ADCs channels are measured using artificial trigger signals in the absence of real events. As a primary acquisition protocol, the acquisition is automatically stopped every 6 hours to take a pedestal run and two calibration runs (one through each back window). Then the normal acquisition is resumed. The movement of the calibration source from the “shielded” parking position to the corresponding window is performed by a stepping motor, which is fully controllable via ECL or TTL signals. These signals are provided by an input/output register VME module controlled by the acquisition software, so the whole acquisition sequence is fully automated.

4. Characterization

To precisely determine the detection properties (efficiency, gain linearity, etc.) of the TPC, it was transported and mounted at the PANTER facility of the Max-Planck-Institut für extraterrestrische Physik (MPE) in Munich in 2002 (Freyberg et al. 2005).

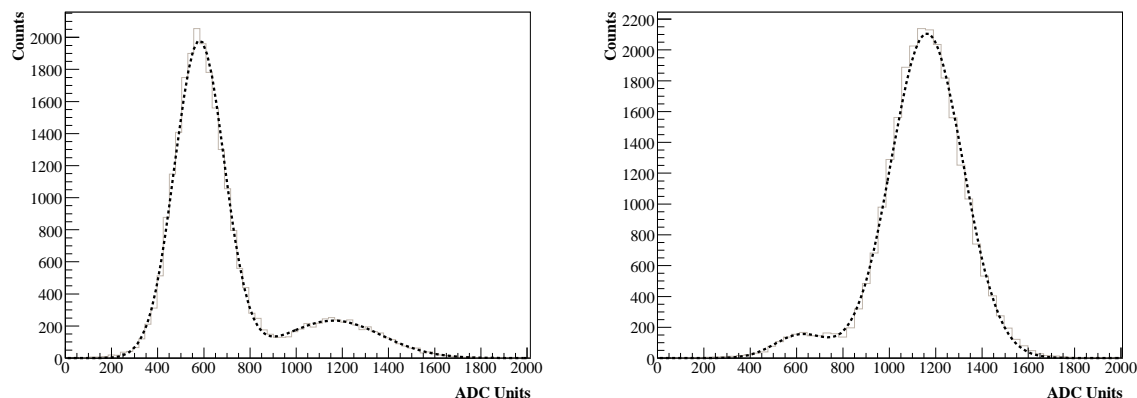


Figure 3. TPC X-ray calibration spectra for an energy of 3 keV and 6.4 keV (Fe-K line, right) measured at the PANTER test facility. In the Fe-K spectrum a second 3.4 keV escape peak is present. In the left spectrum, the bremsstrahlung continuum appears at higher energies in addition to the main peak. The presence of a small amount of bremsstrahlungs background can be deduced from the counts to the left of the peak. In both figures the line shows the combined fit of the peaks plus background.

This facility, designed for the calibration and characterization of X-ray telescopes, provides a parallel X-ray beam with a very accurately calibrated energy and intensity. The data obtained in this facility have been used to determine the efficiency of the TPC, as well as other experimental parameters such as the energy resolution and the linearity of the detector response over the whole energy range of interest. These calibration data have also been used to determine the efficiency loss in the off-line analysis of the data, in particular the energy dependence of the off-line cuts which are applied to reduce the background.

The efficiency curve of the detector has been determined by comparing the counts detected in each corresponding run with the expected rate deduced from the calibrated PANTER detector. The energies provided by PANTER were: 0.3, 0.9, 1.5, 2.3, 3.0, 4.5, 6.4, and 8.0 keV. The beam was “contaminated” by a bremsstrahlung continuum for the low energy cases (from 0.34 up to 3 keV) and the chamber spectra show the presence of a small amount of background. In the case of high energies (from 4.5 up to 8 keV), a second peak due to escape from the argon gas also appears; hence the precise counts corresponding to the main peak have been extracted by means of Gaussian line-shape fits to the measured spectra. Examples of such fits are given in figure 3. The results of these analyses are illustrated in figure 4. The points represent the experimental values and the lines are the theoretical computations. The dark grey line represents the expected fraction of photons passing through the windows and being absorbed somewhere in the sensitive gas volume of the chamber. It is therefore a theoretical (and optimistic) prediction for the efficiency of the detector, taking into account the two main physical effects, i.e., the window transmission and the gas opacity to the incident X-rays. The window transmission contribution is singled out by the upper light grey line (Henke

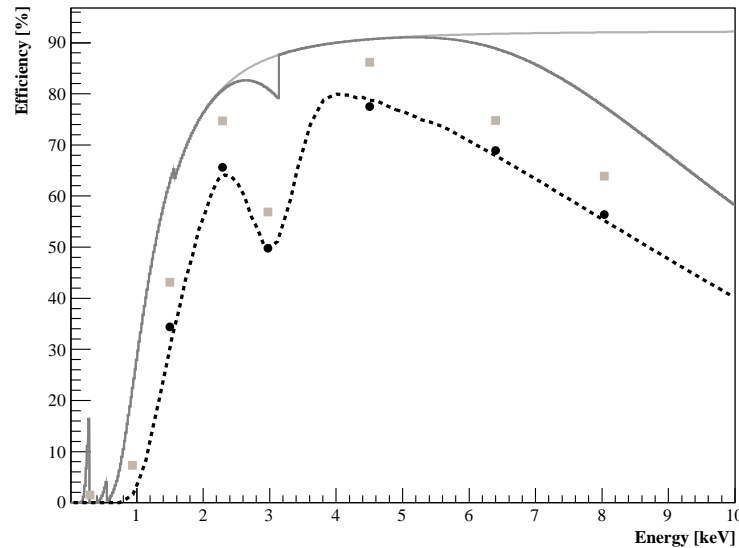


Figure 4. Experimental measurements of the TPC efficiency, before (grey squares) and after (black points) the off-line analysis cuts are applied to the data. The upper light grey line represents the theoretical computation of the window transmission, while the dark grey line includes also the opacity of the gas in the chamber. The black dashed line is the analytical function used to interpolate the experimental points in the final analysis.

et al. 1993), so one can easily see the contribution of both effects separately.

The experimental measurements (grey squares) for each tested PANTER energy closely follow the values expected by the window transmission computation for energies below 3 keV, lying below the grey line for energies above 3 keV due to the presence in the chamber of non point-like events (partial or split energy depositions), which are rejected in the off-line analysis. This loss of efficiency, in agreement with Monte Carlo simulations, is acceptable because of the high background reduction obtained by this approach.

The final off-line analysis (black points) produces an additional loss of efficiency of about 5 to 10 % depending on the energy. The black line is an analytical function used to interpolate the measured efficiencies. By multiplying this function with the expected solar axion spectrum, we obtain an overall detection efficiency of 62% for photons coming from conversion of solar axions. The PANTER data show also the linearity of the TPC response. The position of the main peak versus energy for each measured PANTER energy point is plotted in figure 5 (left), and this verifies the linearity of the detector gain. The points of each set (two different atmospheric pressures) closely follow a straight line, so the linearity of the chamber response has been demonstrated down to the lowest tested X-ray energies.

The run with the lowest available PANTER energy, 0.3 keV, proved that the TPC was sensitive to these energies, although with a very low efficiency (for this run a special

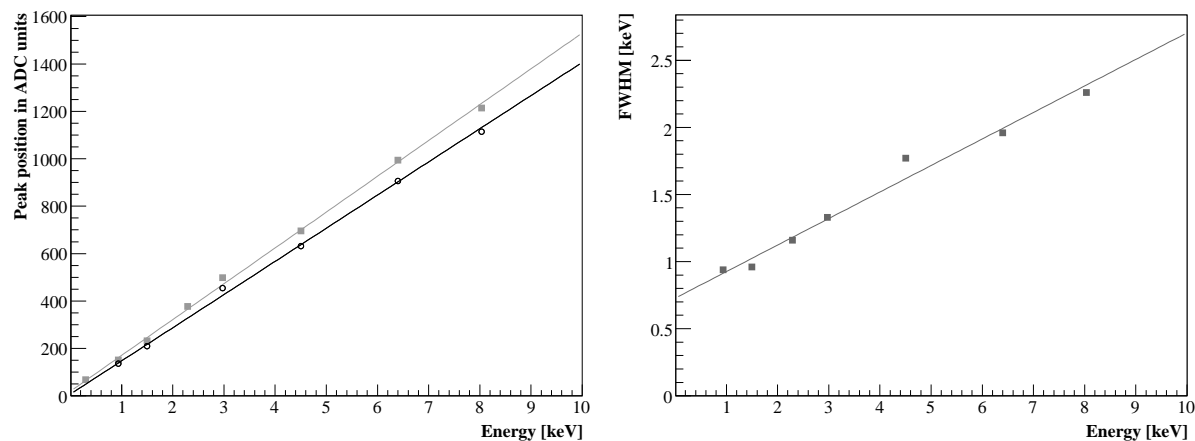


Figure 5. Left: Peak position in arbitrary ADC units versus incident photon energy. The black points and the grey points were taken from two different data sets, showing the variation of the detector gain due to different atmospheric conditions. Right: Measurements of the energy resolution of the TPC detector in terms of full width at half maximum (FWHM) of the photo-peak.

lower trigger threshold was set in the acquisition electronics). The linearity of the detector response is also preserved down to these low energies. Finally, the TPC energy resolution can be also extracted from these data. Figure 5 (right) shows the resolution in terms of Full Width at Half Maximum (FWHM) versus energy.

5. Data Treatment

The first level data treatment of the CAST TPC is focused on the identification of the almost point-like energy depositions produced by the low energy X-rays in the conversion volume of the chamber. Figure 6 shows examples of such depositions for a background event (left) and for an X-ray (right). The plots on the top display the time evolution of the charge pulse generated in each wire as recorded by the flash-ADCs for the row of anodes, while on the bottom the same is shown for the row of cathode wires. The very characteristic profile of an X-ray event provides the framework for a selective analysis.

A first characterization of these raw data generated by the flash-ADCs is performed depending on the spread of the signal. For analysis purposes, a “cluster” is defined as a set of charge pulses (hits) gathered on several contiguous anode wires (anode cluster) as well as on several contiguous cathode wires (cathode cluster) ¶. It has been proven experimentally that X-rays of the energies of interest in our chamber normally produce a single-cluster event firing between 1 and 3 anode wires and between 2 and 8 cathode wires with a time difference between contiguous hits less than 50 ns (see figure 6). The

¶ For analysis purposes we distinguish clusters of anode hits and clusters of cathode hits separately. Obviously, events containing one single physical cluster must contain one anode cluster and one cathode cluster.

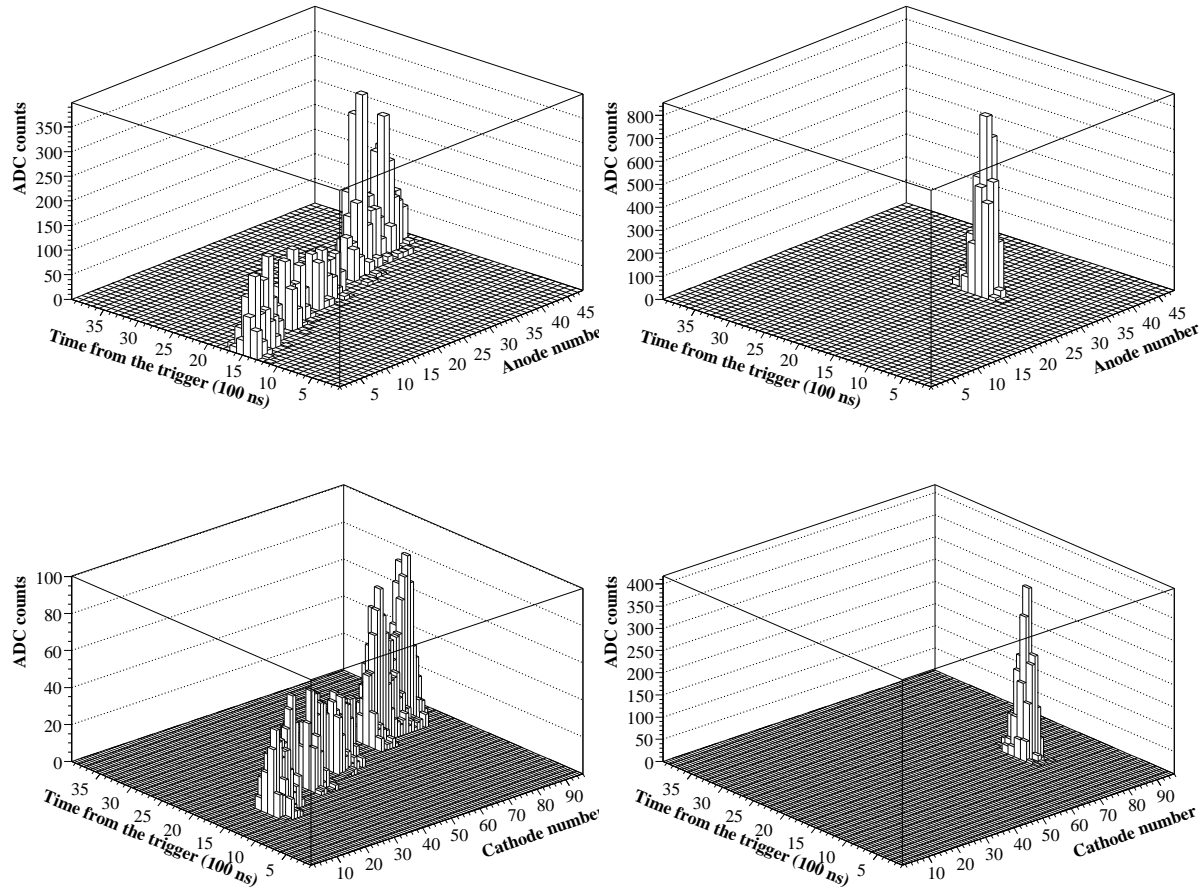


Figure 6. Time evolution of the charge pulse generated in each wire as recorded by the flash-ADCs. Top (bottom) plots correspond to what is collected in the anode (cathode) wires. On the left a background event is plotted, while on the right a X-ray like event is shown.

spread of the anode signal is mainly due to the diffusion of the electron cloud along the drift distance and to a lesser extent to the initial energy deposition (higher energies give larger initial ionization clouds). The larger spread in the cathode wires is due to the development of the avalanche process along the sense (anode) wires. In addition, to be considered as a cluster, the total charge must exceed a minimum charge threshold. This is done to avoid the improbable effect of correlated noise in contiguous wires producing spurious clusters that would affect the efficiency. Therefore, the entire information for one raw data event can now be reduced to a small set of numerical parameters, including:

- Number of clusters in the event and whether they are in the anode or cathode wire plane. This number provides information on the signal spread.
- Multiplicity of every cluster, i.e., number of hits comprising the cluster.
- Total cluster charge calculated by adding up the charge of every hit comprising the cluster.

Table 1. List of software cuts applied to the CAST TPC data.

cut	condition
anode multiplicity	number of anode hits between 1 and 3 (both inclusive)
cathode multiplicity	number of cathode hits between 2 and 8 (both inclusive)
anode–cathode time difference	time between anode and cathode cluster in the range -0.15 to $0.02 \mu\text{s}$
no saturation	no hit reaching the upper part of the flash-ADC dynamical range
anode–cathode charge ratio	around 1.85, but slightly energy dependent
fiducial cut	only events whose 2-D coordinates are inside the windows facing the magnet bores

- Cluster position calculated by the charge-weighted mean of the position (wire number) of every hit comprising the cluster.
- Cluster time (related to the trigger) calculated by the charge-weighted mean of the times of every hit composing the cluster.

Next, a set of software cuts are applied to reject events that are clearly not produced by X-ray interactions. The first and most important one is the requirement that there is one single anode cluster and one single cathode cluster. It is then straightforward to match both of them to get the 2-dimensional position of the point-like event. A detailed list of further conditions required on the cluster properties is given in table 1. This set of cuts is a minimal choice designed to reject a large portion of background events while minimally reducing the efficiency of the detector. Typically its application reduces the background by approximately two orders of magnitude with respect to the raw trigger rate. The loss of efficiency generated by the software cuts has been carefully measured using the PANTER data as described above, in particular regarding the loss of X-rays events with split energy deposition (2 or more cluster events) due to the argon escape peak.

The cluster energy is obtained by adding up the calibrated flash-ADC output for every constituent hit. In 2003 data taking, the gain variations of the gas in the chamber were characterized by continuous measurements of its pressure and temperature. In 2004 the introduction of a stepping motor allowed fully automated calibration runs with a ^{55}Fe source every 6 hours as described in section 3. Therefore, measurements of the gas gain for each window were performed and used to calibrate the flash-ADCs. Figure 7 shows the evolution of the measured gain during the 2004 data taking period.

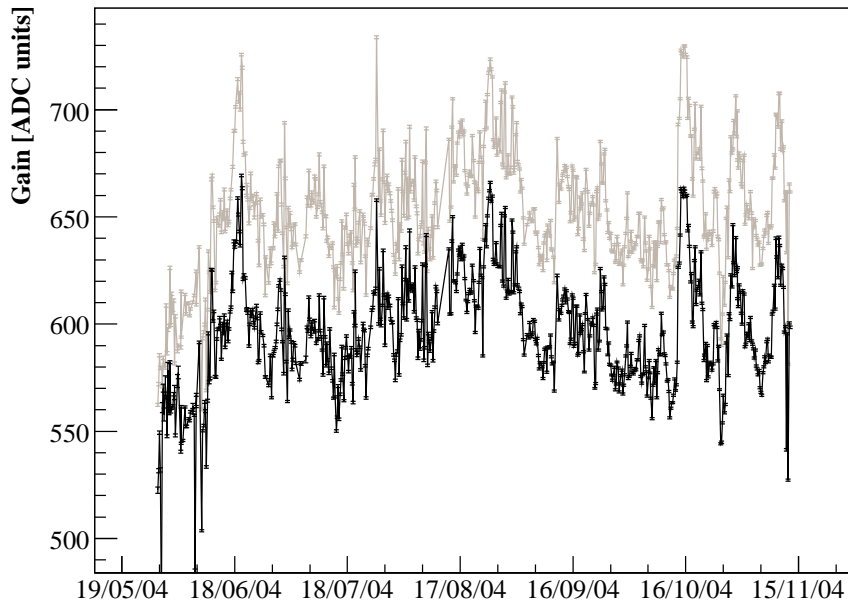


Figure 7. Gain evolution during 2004 data taking in the two windows of the TPC, given by the ADC channel corresponding to the position of the Mn-K α line of an ^{55}Fe calibration source.

A difference of the gain values for the two windows was observed and this was taken into account in the data analysis. This difference results from geometrical imperfections in the wire arrangement that produce a gain drift along the anodes. Slight wire-to-wire variations due to mechanical imperfections or adjustments of the preamplifiers were also observed and further corrected by calibrating the gain of every wire independently. The energy spectrum of the events that have passed all cuts is then computed for two distinct classes: the first for all X-ray events collected during the axion-sensitive periods (when the magnet is pointing towards the Sun) and the second for the background spectrum. The X-rays coming from conversion of solar axions should appear as an excess in the first spectrum when compared to the second one.

6. Detector Performance

6.1. 2003 Data Taking

Although the data taking period of 2003 lasted for about 6 months, much of this time corresponds to commissioning operation, periods when data taking was temporarily stopped due to specific technical interventions in the experiment (related for example to the problems with the mechanical structure) or in the TPC itself (replacement of leaky windows, for example) or periods when data was taken but they did not pass the quality requirements regarding homogeneity of operation, due to the relatively frequent

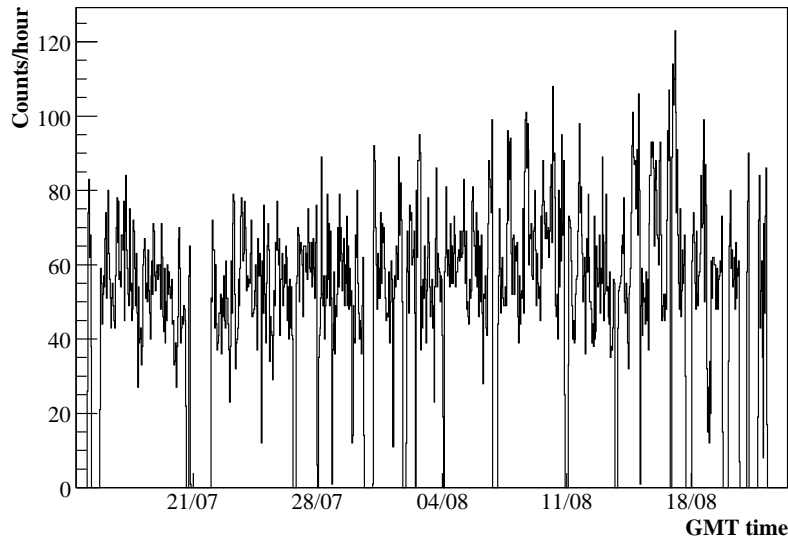


Figure 8. Measured count rate in the 3 to 7 keV energy range in units of counts per hour as observed by the TPC detector during July and August 2003 after applying cuts.

interruptions in the experiment, mainly due to magnet quenches, and to a lesser extent to episodes of electronic noise pick-up in the detector.

As a result, the effective amount of data qualified for analysis obtained by the TPC in 2003 was ~ 783 h, all of them concentrated in the months of July and August. Out of these data, ~ 63 h (9% of the total) were taken when the magnet was tracking the Sun. The stability and continuity of operation of the detector during this time can be appreciated in figure 8, where the counting rate is represented. Regarding the performance of the TPC setup, the main problem preventing a continuous operation beyond the period signaled was the deterioration of the leak tightness of the X-ray windows beyond the magnet vacuum requirements. This strongly motivated the development of the differential pumping system previously described, and its installation at the beginning of the 2004 data taking period.

On the other hand, during 2003 the TPC operated with a reduced shielding consisting only of the innermost copper cage previously presented and the N_2 flow. With this reduced shielding, the observed background suffered from a strong dependence on the magnet position, caused by the relatively large spatial movements at the far end of the magnet, which resulted, as previously mentioned, in appreciably different environmental radioactivity levels. This effect prevented a straightforward, background-subtracting, analysis. To correct for this systematic effect an effective background spectrum was constructed only from the background data taken in magnet positions where Sun tracking had been performed and this was weighted accordingly with the relative exposure of the tracking data.

In practice, we distinguish the differential spectrum of the complete background

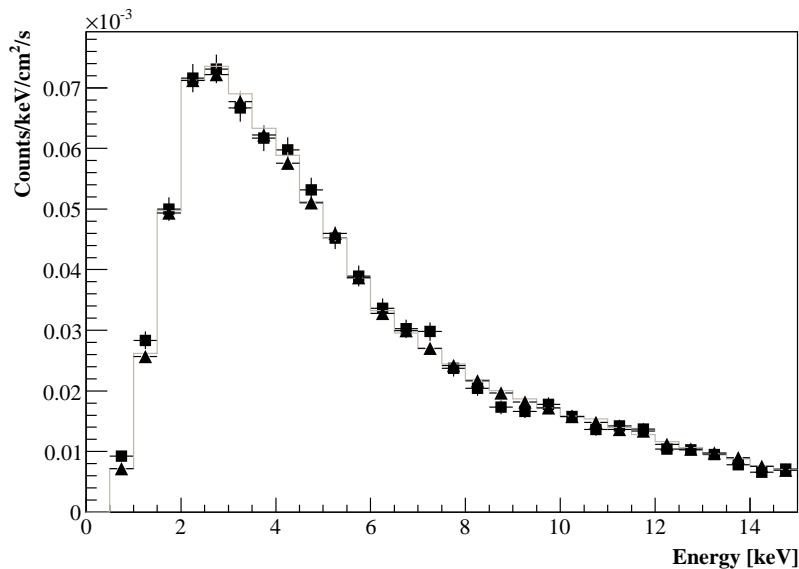


Figure 9. Three different spectra are shown: the total measured background spectrum (triangles), the weighted background spectrum (squares), and the tracking spectrum (solid line, see also Andriamonje et al. 2007).

data, dN_b/dE from the partial background spectra $(dN_b/dE)_i$ corresponding to the data gathered in the “cell” i of the magnet position plane (azimuth-altitude). The effective background spectrum to be subtracted from the tracking data that will not suffer from this systematic effect regarding magnet position was defined as:

$$\left(\frac{dN_b}{dE}\right)_{\text{eff}} = \frac{\sum_i (dN_b/dE)_i \epsilon_i}{\sum_i \epsilon_i} \quad (1)$$

where ϵ_i is the exposure of the tracking data for magnet positions in the cell i . The more cells used, the smaller the systematic error will be when considering the effective background, but on the other hand the higher the statistical errors due to the poor available statistics in each of the cells. For the 2003 data, it was seen that a grid of 3×3 cells is sufficient to reduce this effect well below the statistical error in the tracking data. In figure 9 both the total background spectrum and the one obtained after the above weighting are shown in comparison to the tracking spectrum.

6.2. 2004 Data Taking

In 2004, with the differential pumping system installed and the general improvements in the CAST experiment, the whole TPC setup worked safely without interruption for the full duration of the data taking period (six months). The collected data are of very high quality, due to the installation of the shielding and the detector stability. Figure 10 shows the rate of filtered events between 3 and 7 keV collected during this period. Data were taken during ~ 151 effective days, of which 9 days ($\sim 6\%$) correspond to axion sensitive conditions.

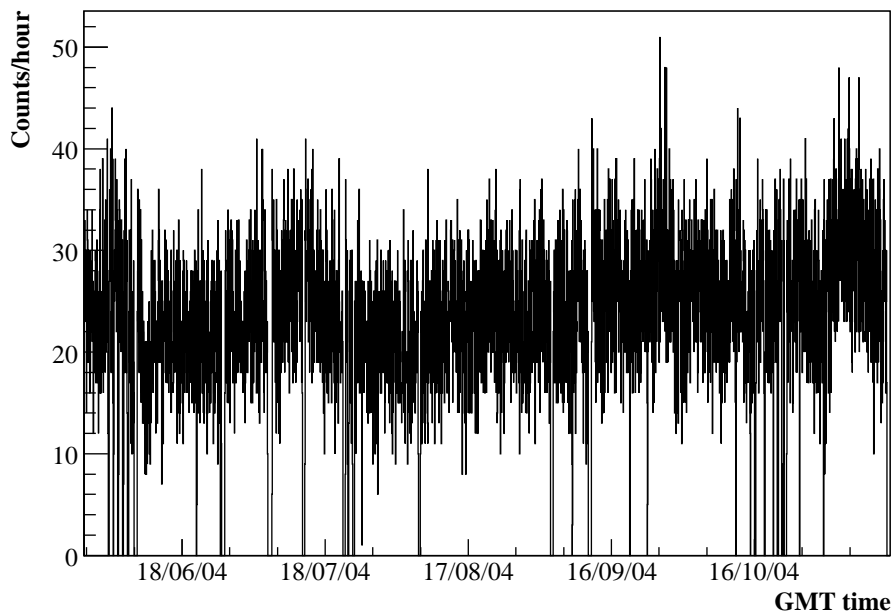


Figure 10. Measured count rate in the 3 to 7 keV energy range in units of counts per day as observed by the TPC detector during 2004 data taking period.

With the shielding installed around the chamber, the TPC background level between 1 and 10 keV was $4.10 \times 10^{-5} \text{ counts cm}^{-2} \text{ s}^{-1} \text{ keV}^{-1}$, a factor of ~ 4.3 below the level reached by the TPC with no shielding. This reduction increases with energy (reduction factor of ~ 6.4 in the 6 to 10 keV range). The observed background energy spectra for both setups with and without shielding are shown in the left panel of figure 11, as well as for an intermediate configuration with only the copper box and N_2 flux.

Regarding the performance of the muon veto installed as part of the shielding, it was observed, as expected, that the events in coincidence with the muon veto are mostly rejected by the software cuts, since the muon leaves a very distinctive signature in the TPC. The amount of events rejected by anti-coincidence with the veto and not previously rejected by the software cuts represent only 4% of the final background. This small population is due to muon-induced events leaving a point-like energy deposit in the TPC, like neutrons produced by the muons in the shielding.

In order to have a better control of the spatial background inhomogeneities, background data were always taken in well defined positions in the experimental hall. For this purpose, an 3×3 x - y grid was defined, where $x(y)$ is the TPC horizontal (vertical) coordinate in the experimental hall. In this way, 9 cells cover the different TPC positions, and the background level was measured in each of them. The right panel of Figure 11 shows the result of the measurements for both the 2003 and 2004 data. During 2003 the TPC was shielded only with the copper box and the N_2 flux and differences in the background rate due to the proximity of a concrete wall are clearly

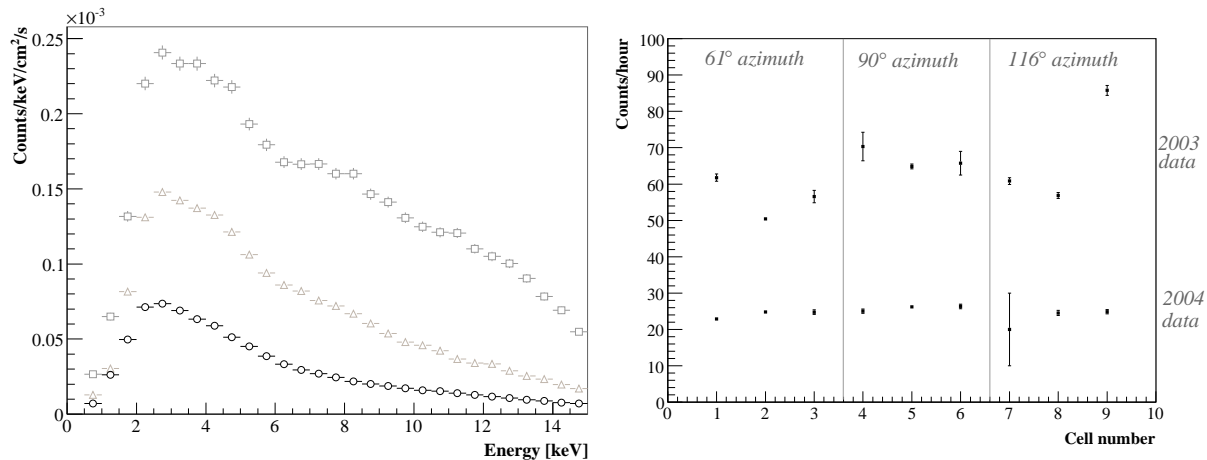


Figure 11. Left: Background spectra for the TPC detector measured under different shielding conditions. Right: Comparison between 2003 (top) and 2004 background data (bottom) measured for different magnet orientations, i.e., different detector location relative to the environment of the experiment area. The cell numbers indicate 3 different horizontal positions and 3 different vertical positions.

seen. On the other hand, for the 2004 data the overall effect of the shielding can be observed, both in the reduction and also in the clear homogenization of the overall background level.

7. Conclusion

The CAST TPC detector, built to search for solar axions, has been presented in detail. A design option of 10 cm maximum drift length with a conventional multi-wire readout plane has been implemented to provide the experimental requirements of high sensitivity to X-rays from the magnet bores. Some innovative features of the detector design include two thin X-ray windows to allow photons coming from the magnet bores to enter the detector with very small losses, a differential pumping system to couple the chamber to the magnet while maintaining the stringent requirements of leak rate towards the magnet vacuum, and a low background shielding built around the detector to reduce the background and to make it more uniform in space. A detailed characterization of the detector in the PANTER facility in Munich has been performed, proving an adequate response linearity, a low energy threshold and an overall (hardware plus software) efficiency of 62% for photons coming from conversion of solar axions. The imaging capabilities of the multi-wire readout enable a high background discrimination which, together with the radio-purity of the detector materials and the detector shielding, results in a background rate of only 4.10×10^{-5} counts $\text{cm}^{-2} \text{s}^{-1} \text{keV}^{-1}$ between 1 and 10 keV. The whole system has been proved to be robust and stable during the full data taking of CAST phase I, allowing for a reliable background subtraction and therefore contributing to the overall CAST limit on axion-photon coupling and mass (Zioutas

et al. 2005).

Acknowledgments

This work has been performed in the CAST collaboration. We thank our colleagues for their support. We would like to express here our gratitude to the group of the Laboratorio de Física Nuclear y Altas Energías of the Zaragoza University for material radio-purity measurements. Furthermore, the authors acknowledge the helpful discussions within the network on direct dark matter detection of the ILIAS integrating activity (Contract number: RII3-CT-2003-506222).

References

- Abbon P, Andriamonje S, Aune S, Dafni T, Davenport M, Delagnes E, de Oliveira R, Fanourakis G, Ferrer Ribas E, Franz J, Gerasis T, Gros M, Giomataris Y, G. I I, Kousouris K, Morales J, Papaevangelou T, Ruz J, Zachariadou K & Zioutas K 2007 *New J. Phys.* this volume.
- Andriamonje S, Aune S, Autiero D, Barth K, Belov A, Beltrán B, Bräuninger H, Carmona J, Cebrián S, Collar J I, Dafni T, Davenport M, Di Lella L, Eleftheriadis C, Englhauser J, Fanourakis G, Ferrer Ribas E, Fischer H, Franz J, Friedrich P, Gerasis T, Giomataris I, Gninenko S, Gómez H, Hasinoff M, Heinsius F H, Hoffmann D H H, Irastorza I G, Jacoby J, Jakovčić K, Kang D, Königsman K, Kotthaus R, Krčmar M, Kousouris K, Kuster M, Lakić B, Lasseur C, Liolios A, Ljubičić A, Lutz G, Luzon G, Miller D, Morales A, Morales J, Ortiz A, Papaevangelou T, Placci A, Raffelt G, Riege H, Rodríguez A, Ruz J, Savvidis I, Semertzidis Y, Serpico P, Stewart L, Vieira J, Villar J, Vogel J, Walckiers L & Zioutas K 2007 *New. J. Phys.* in preparation.
- Andriamonje S, Aune S, Barth K, Belov A, Beltrán B, Bräuninger H, Carmona J, Cebrián S, Collar J I, Dafni T, Davenport M, Di Lella L, Eleftheriadis C, Englhauser J, Fanourakis G, Ferrer-Ribas E, Fischer H, Franz J, Friedrich P, Gerasis T, Giomataris I, Gninenko S, Gómez H, Hasinoff M, Heinsius F H, Hoffmann D H H, Irastorza I G, Jacoby J, Jakovčić K, Kang D, Königsman K, Kotthaus R, Krčmar M, Kousouris K, Kuster M, Lakić B, Lasseur C, Liolios A, Ljubičić A, Lutz G, Luzon G, Miller D, Morales A, Morales J, Ortiz A, Papaevangelou T, Placci A, Raffelt G, Riege H, Rodríguez A, Ruz J, Savvidis I, Semertzidis Y, Serpico P, Stewart L, Villar J, Vogel J, Walckiers L & Zioutas K 2007 *J. Cosmol. Astropart. Phys.* submitted.
- Bosch E R 2003 Vol. 50 IEEE Transaction on Nuclear Science.
- Brun R & Rademakers F 1996 *Nucl. Instrum. Methods Phys. Res., Sect. A* **389**, 81–86.
*<http://root.cern.ch/>
- Dumont G 2004 Technical Note CERN-SC-2004-027-RP-TN CERN, Geneva.
- Freyberg M J, Bräuninger H, Burkert W, Hartner G D, Citterio O, Mazzoleni F, Pareschi G, Spiga D, Romaine S, Gorenstein P & Ramsey B D 2005 *Experimental Astronomy* **20**, 405–412.
- Henke B L, Gullikson E M & Davis J C 1993 *Atomic Data and Nuclear Data Tables* **54**(2), 181–342.
*<http://www-cxro.lbl.gov>
- Kuster M, Bräuninger H, Davenport M, Englhauser J, Fischer H, Franz J, Friedrich P, Hartmann R, H. H F, Hoffmann D, Hoffmeister G, Joux J N, Kang D, Königsman K, Kotthaus, R. Papaevangelou T, Lasseur C, Lippitsch A, Lutz G, Strüder L, Vogel J & Zioutas K 2007 *New J. Phys.* this volume.
- Ruz J & Luzón G 2006 in ‘Proceedings of the 9th International Conference on Topics in Astroparticle and Underground Physics 2005 (TAUP05)’ Vol. 39 Journal of Physics, Conference Series pp. 191–193.
- Sikivie P 1983 *Phys. Rev. Lett.* **51**, 1415–1417.

- Zioutas K, Aalseth C E, Abriola D, Avignone III F T, Brodzinski R L, Collar J I, Creswick R, Gregorio D E D, Farach H, Gattone A, Guérard C K, Hasenbalg F, Hasinoff M, Huck H, Liolios A, Miley H S, Morales A, Morales J, Nikas D, Nussinov S, Ortiz A, Savvidis E, Scopel S, Sievers P, Villar J A & Walckiers L 1999 *Nuclear Instruments and Methods in Physics Research A* **425**, 480–487.
- Zioutas K, Andriamonje S, Arsov V, Aune S, Autiero D, Avignone F T, Barth K, Belov A, Beltrán B, Bräuninger H, Carmona J M, Cebrián S, Chesi E, Collar J I, Creswick R, Dafni T, Davenport M, di Lella L, Eleftheriadis C, Englhauser J, Fanourakis G, Farach H, Ferrer E, Fischer H, Franz J, Friedrich P, Geralis T, Giomataris I, Gninenko S, Goloubev N, Hasinoff M D, Heinsius F H, Hoffmann D H H, Irastorza I G, Jacoby J, Kang D, Königsmann K, Kotthaus R, Krčmar M, Kousouris K, Kuster M, Lakić B, Lasseur C, Liolios A, Ljubičić A, Lutz G, Luzón G, Miller D W, Morales A, Morales J, Mutterer M, Nikolaidis A, Ortiz A, Papaevangelou T, Placci A, Raffelt G, Ruz J, Riege H, Sarsa M L, Savvidis I, Serber W, Serpico P, Semertzidis Y, Stewart L, Vieira J D, Villar J, Walckiers L & Zachariadou K 2005 *Phys. Rev. Lett.* **94**(12), 121301–+.